Colloids and Surfaces B: Biointerfaces 234 (2024) 113751

Contents lists available at ScienceDirect

Colloids and Surfaces B: Biointerfaces

journal homepage: www.elsevier.com/locate/colsurfb

Breast adenocarcinoma cells adhere stronger to brain pericytes than to endothelial cells

Katalin Csonti [a,b,c], Csilla Fazakas [a], Kinga Molnár [a], Imola Wilhelm [a,d], István A. Krizbai [a,d], Attila G. Végh [a,*]

[a] HUN-REN BRC, Szeged, Institute of Biophysics, Hungary
[b] Doctoral School of Physics, University of Szeged, Szeged, Hungary
[c] Semilab Semiconductor Physics Laboratory Co. Ltd., Budapest, Hungary
[d] Institute of Life Sciences, Vasile Goldiş Western University, Arad, Romania

ARTICLE INFO

Keywords:
Single-cell force spectroscopy
Cell adhesion
Human brain endothelial cells
Human brain pericytes
Brain metastasis formation
Breast adenocarcinoma

ABSTRACT

Most of the malignancies detected within the brain parenchyma are of metastatic origin. As the brain lacks classical lymphatic circulation, the primary way for metastasis relies on hematogenous routes. Dissemination of metastatic cells to the brain implies attachment to the luminal surface of brain endothelial cells, transmigration through the vessel wall, and adhesion to the brain surface of the vasculature. During this process, tumor cells must interact with brain endothelial cells and later on with pericytes. Physical interaction between tumor cells and brain vascular cells might be crucial in the successful extravasation of metastatic cells through blood vessels and later in their survival within the brain environment. Therefore, we applied single-cell force spectroscopy to investigate the nanoscale adhesive properties of living breast adenocarcinoma cells to brain endothelial cells and pericytes. We found target cell type-dependent adhesion characteristics, i.e. increased adhesion of the tumor cells to pericytes in comparison to endothelial cells, which underlines the existence of metastatic potential-related nanomechanical differences relying partly on membrane tether dynamics. Varying adhesion strength of the tumor cells to different cell types of brain vessels presumably reflects the transitory adhesion to endothelial cells before extravasation and the long-lasting strong interaction with pericytes during survival and proliferation in the brain. Our results highlight the importance of specific mechanical interactions between tumor cells and host cells during metastasis formation.

1. Introduction

Breast cancer (BC) is the most common malignancy in women and the second major cause of death (after lung cancer) [1,2]. Metastasis is a major cause of morbidity and mortality in breast cancer patients [1,3]. The five-year relative survival in local invasive breast cancer patients is 98.1%, while it is only 26% in patients with distant metastases [1]. The biological underpinnings of tumor metastasis remain the least understood aspect of cancer biology, and elucidating the underlying mechanisms driving metastasis is essential [4]. Metastasis involves sequential invasion into the blood vessels or lymph nodes from the primary site and subsequent extravasation into secondary sites [5]. Tumor cell dissemination through the blood is thought to be the main route of metastasis [6]. Although it might appear difficult, tumor cells can reach the blood circulation, survive shear stress, escape immune surveillance, avoid detachment-induced cell death, extravasate at distant sites and finally establish metastasis [6,7]. During this multistep process, tumor cells might reduce their adhesiveness to the primary tumor to be able to escape it, and they increase their adhesiveness again once they reach the target host cell surface so that they can adhere to it [8,9].

Brain metastases (10 to 30% of all breast cancer-related metastasis [3]) represent one of the incurable end stages of BC. BC cells that preferentially metastasize to the brain frequently belong to the triple-negative subgroup [3]. Developing effective or preventive treatments is hampered by a lack of knowledge of the molecular mechanisms driving brain metastasis. Current treatments are palliative with poor efficacy and include surgical resection, radiotherapy, chemotherapy and targeted therapies. Even if currently available therapeutic protocols may be successful at the beginning, these types of tumors are highly drug-resistant, and recurrence is a frequent phenomenon [10]. Most

* Corresponding author.
E-mail address: veghattilagergely@brc.hu (A.G. Végh).

https://doi.org/10.1016/j.colsurfb.2024.113751
Received 5 October 2023; Received in revised form 22 December 2023; Accepted 7 January 2024
Available online 11 January 2024

therapeutic drugs that are effective in treating primary tumors fail to treat brain metastases because the blood–brain barrier (BBB) limits the ability of drugs to enter and evoke tumor cell death, rendering the brain a "sanctuary site"[11,12]. The BBB, the most important function of the dynamic and complex neurovascular unit, is constructed to build an effective shield against larger molecular substances and objects that may harm brain function and allow only necessary small substances present in the blood to pass through [1]. As a highly selective interface between the blood and the brain, it is indispensable to protect the brain parenchyma from the influence of circulatory factors and regulate and maintain the stability of the internal environment [13]. Without the BBB, the central nervous system is vulnerable to toxins, pathogens, and ion dysregulation, leading to dysfunction and degeneration [14]. It plays a vital role in regulating the trafficking of solutes, fluid, and cells at the blood—brain interface [15]. Damage to the BBB is a major part of the pathophysiological process of many nervous system diseases [16,17,18]. The BBB is one of the most important properties of the neurovascular unit built up predominantly of three cell types, which are the building blocks of the microvascular system of the brain: endothelial cells, astrocytes and pericytes [14,18,19]. The most important are endothelial cells, which are connected by tight junctions and form the mechanical part of the barrier. Endothelial cell tight junctions limit the paracellular flux of hydrophilic molecules across the BBB [19]. Pericytes are vascular mural cells that are close to brain endothelial cells, and their processes cover ~90% of the length of the capillary bed [20]. Pericytes themselves help to preserve BBB integrity and decrease the paracellular permeability of endothelial cells by enhancing the formation of tight junctions and maintaining low levels of transcytosis in the brain endothelium [14]. During brain metastasis formation, BC cells encounter both cerebral endothelial cells and pericytes. Before extravasation, the first step for circulating tumor cells prior to forming brain metastasis is firm adhesion to the endothelial cells of the brain vasculature [21]. Transmigration of BC cells through the brain endothelium is a key event in the pathogenesis of brain metastasis [12]. After reaching the brain parenchyma, BC cells attach to the vessels and come in contact with pericytes which hold prometastatic properties [22]. The malignant phenotype and metastatic potential of cancer cells might be correlated with their elastic properties [8].

Atomic force microscopy (AFM) is a high-resolution force tool that can be used to investigate the morphology of a sample and quantitatively measure its mechanical properties at atomic resolution [23]. The system uses a soft cantilever that can be chemically modified to transform itself into a cell probe. Thus, living cells might be used to probe the interaction with either surfaces or other living cells, providing sensitive force-, position-, and time-resolved adhesion measurements [24–26].

The present study compares the adhesive properties of breast adenocarcinoma cells to confluent layers of brain endothelial cells and pericytes. AFM based single-cell force spectroscopy was applied to investigate the details of the adhesive strength of parental and brain-seeking metastatic tumor cells upon contact with brain endothelial cells and pericytes.

2. Materials and methods

2.1. Cell culture

Human brain endothelial (HCMEC/D3, – originating from the laboratory of Pierre-Olivier Couraud, INSERM U567, Institut Cochin, Paris, France [27]) cells were grown on rat tail collagen-coated (type I collagen) and cultured in EBM-2 medium (Lonza) supplemented with EGM-2 MV (Lonza) until confluence was reached. Endothelial cells between passage numbers 30 and 36 were used for force spectroscopy measurements. Their characterization regarding expression of specific brain endothelial markers was performed by western blot and immunofluorescence staining (Supplementary Fig. S1).

Human brain vascular pericytes (abbreviated as HBVP; obtained from ScienCell Research Laboratories, Carlsbad, CA, USA; Catalog No. 1200) were cultured on poly-L-lysine-coated dishes in Pericyte Medium (PM; ScienCell Research Laboratories) supplemented with 5% FBS (Sigma-Aldrich, St. Louis, MO, USA) and penicillin/streptomycin solution (P/S; ScienCell Research Laboratories) and used between passage numbers 2 and 6. The HBVP cells used in these experiments were from two different lots (lot. no: 19275 and lot. no:27288). Characterization of specific pericyte markers was performed by western blots analysis (Supplementary Fig. S1).

The human triple negative breast cancer cells – the parental cell line MDA-MB-231-TGL (MDA-231-HSV1-TK/GFP/Fluc, abbreviated as TGL) and the brain-seeking MDA-MB-231-BrM2 (abbreviated as BrM2) cells – were obtained from Dr. Joan Massagué at Memorial Sloan Kettering Cancer Center (New York, NY, USA). The TGL and BrM2 cells used for the measurement were cultured in DMEM (Gibco, Thermo Fisher Scientific) containing 10% FBS (Gibco, Thermo Fisher Scientific). The cells were authenticated by analysis of highly variable short tandem repeat (STR) markers using Applied Biosystems™ GeneMapper™ Software 6 (Thermo Fisher Scientific).

All cell types were regularly tested for mycoplasma infection with a MycoAlert Mycoplasma Detection Kit (Lonza, Basel, Switzerland) and were maintained at 37 °C in a humid incubator with 5% CO2 in air.

2.2. Adhesion assays

Adhesion assays were carried out as previously described [28]. HCMEC/D3 or HBVPs were seeded into 24-well plates and cultured until confluent. TGL or BrM2 cells were labeled with 1 μM Oregon Green (Thermo Fisher Scientific) for 15 min in serum-free DMEM at 37 °C. Labeled cells were washed, and complete media was given to cells for 30 min before harvesting. Breast cancer cells were seeded at 5 * 10^4/well. Tumor cells were left to adhere for 60 min to endothelial cells or pericytes, after which cells were washed with PBS and fixed with 4% (w/v) paraformaldehyde for 10 min at room temperature followed by three washing steps with PBS. Adherent cells were imaged by a Nikon epifluorescence microscope with a 10x objective, 5 images/well, and counted using the ImageJ/Cell Counter plugin.

Cell culture for force measurements.

The TGL and BrM2 cells used for the force measurements were cultured in DMEM (Gibco) containing 10% FBS (Gibco). Before single-cell force spectroscopy experiments, tumor cells were fluorescently labeled with 1 μM calcein-AM (Sigma) dye in serum-free DMEM for 20 min, after which they received serum-containing media for 20 min.

Human brain endothelial (HCMEC/D3) cells were grown on rat tail collagen-coated (type I collagen) cell culture dish lids separated by the silicone walls of a four-segment Ibidi chamber (Fig. S2). Cells were cultured in EBM-2 medium (Lonza) supplemented with EGM-2 MV (Lonza) until confluence was reached. Human brain microvascular pericytes (HBVPs) were grown on poly-L-lysine-coated dish lids separated by the silicone walls of a four-well Ibidi chamber. In the Ibidi chamber, there was an empty well where the tumor cells (TGL or BrM2) were attached to the functionalized cantilever in all cases (Fig. 1). This was followed by the chamber part containing HCMEC or HBVP cell

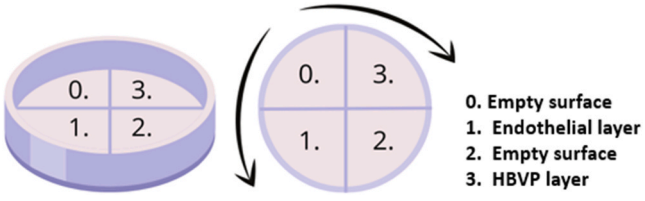

Fig. 1. Schematic representation of the experimental setup. After removal of the silicone walls separating the wells, the four different surfaces were consecutively probed with a tumor cell, moving the cantilever sequentially clockwise or counterclockwise.

layers.

The measurements were made after removal of the Ibidi chamber in different (clockwise or counterclockwise) directions. Only those were included in the final analysis where the results were not dependent on the sequence of effectuation (A representative example and details on the measurement can be seen on the Supplementary material and Fig. S3, S4). All experiments were conducted in serum-free Leibovitz medium at 37 °C within 2 h after the cells were removed from the incubator. According to our experience, they preserve their viability far beyond this period.

2.3. Atomic force microscopy

All force spectroscopy experiments were performed with an Asylum Research MFP-3D atomic force microscope (Asylum Research, Santa Barbara, CA; IgorPro 6.32 A control software, Wavemetrics) mounted on top of a Zeiss Axiovert 200 optical microscope for optical positioning. The bracket on which the tumor cell is immobilized is located on a silicon nitride probe with three tipless cantilevers, the middle one used for measurements. This cantilever has a normal spring constant of 30 pN/nm and a resonant frequency of 10 kHz. All probes were calibrated before the experiment using the thermal noise method [29] and the Sader method [30]. The data from the measurements were evaluated and visualized in MATLAB (MathWorks).

2.4. Single-cell force spectroscopy

Cancer cells were immobilized at the very end of the tipless cantilever using a concanavalin-A-mediated linkage, which is described in detail elsewhere [31,32]. Briefly, first, a tumor cell suspension was pipetted onto the Petri dish, and then a tumor cell that has not yet adhered to the surface of the culture dish was selected. The size and morphology were checked using an optical microscope. The cantilever was pressed onto the selected tumor cell until the force required for immobilization was reached, and the adhesion force between the cell and the cantilever was stronger than that between the probe cell and the culture dish. The position of the immobilized tumor cell on the cantilever was monitored using an optical microscope before, during, and after the measurement (Fig. S3). During a force measurement cycle, a cancer cell immobilized at the end of a tipless cantilever was brought into contact with surface-adherent endothelial cells or pericytes. The schematic representation and the annotations for the extracted parameters can be found in Fig. 2.

In a typical AFM force–distance measurement, the tip is brought toward and retracted from the cell surface; its interaction forces are monitored as a function of the cantilever's displacement, and they are recorded as force–displacement curves. As a result, a plentitude of quantitative information can be extracted from these curves regarding cell elasticity and adhesiveness [8]. The principle of operation is to monitor the forces acting between the tip and the sample surface. The tip–sample interaction forces cause the cantilever to deflect, which is recorded via a laser beam focused on the cantilever's free end and reflected onto a position-sensitive photodiode [25]. Upon approach, the tip and the sample surface are first far enough apart not to interact, resulting in null force. Decreasing the tip–sample distance results in diverse long-range and short-range repulsive or attractive interactions (for example, electrostatic or van der Waals forces) until the tip makes contact with the surface. As the tip is further pushed against the sample, it induces an upward deflection of the cantilever. When a predefined force is reached, the motion of the tip is halted and reversed. As the tip is moved upward, the cantilever relaxes and then often deflects downward owing to adhesive forces between the tip and sample. Finally, the tip–surface contact ruptures, and the cantilever returns to its zero-force position [25].

At each force measurement cycle, the cell-loaded cantilever approached the endothelial or pericyte layer until the preset deflection was reached (maximal load of 2 nN), after which it was pulled back to the initial position. One set of measurements was completed within two hours. Our measurements were designed in such a way that the adhesion of the same probe cell to the substrate layers (endothelial cells and pericytes) was tested to increase the accuracy of the system. Further details about the experimental setups can be found in the Supplementary Material.

The stress relaxation percentage was calculated as the force sensed by the cantilever at the end of the dwell time reported to the maximal load (as an intuitive approach, 100% would be maximal relaxation-totally plastic material; 0% would be lack of relaxation-perfectly elastic material). The elastic index is calculated as a percentage of the ratio of the loading work and the amount of work the cell can still exert during cantilever retraction (0% in the case of a perfectly plastic material and 100% in the case of a perfectly elastic material). Values of maximal **adhesion force** were considered as the difference between the force at the maximal downward deflections of the cantilever compared to the initial value during the noncontact state [26]. **Rupture size** was

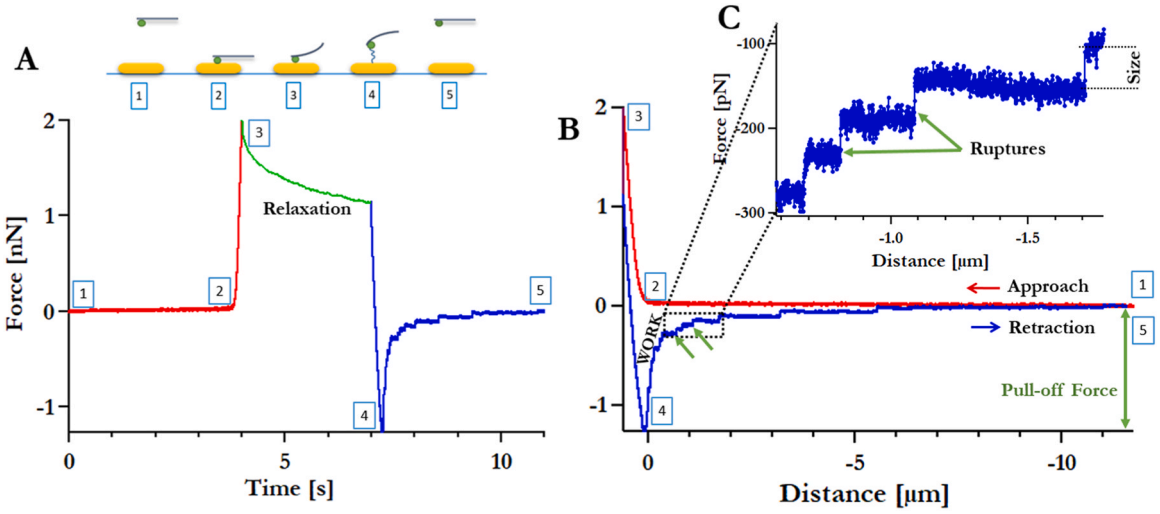

Fig. 2. Schematic representation of the force measurement cycle. Immobilized tumor cells at the very end of the tipless cantilever pushed to the tested cell layers. Recorded force versus time (panel A) and force versus distance (panel B) curves using AFM-based force spectroscopy. Panel C represents the magnified area with the detected rupture events marked with green arrows.

calculated as a level difference of the mean of 5 points before and after the place of occurrence [26] (see panel C on Fig. 2). **Rupture length** represents the distance from the place of the initial contact point between the two cells and the position of the last point before an identified disruption event. The distribution of rupture size and length are represented by histograms showing the probability of finding a given value within the whole data population calculated for each cell type [26]. **Rupture Force** is calculated as the actual amount of exerted force at the occurrence of a rupture event. All the mentioned parameters were extracted and calculated with the help of a custom written MATLAB (MathWorks)-based algorithm. If not stated otherwise, the results presented by box plots include the median (red line) value of the population, the upper and lower edges of the box are the first upper and lower quartiles, and the whiskers show 75% and 25% of the values. Outliers are represented by red plus signs (+) on box plots, where the exclusion criterion was that the value was situated outside 1.5-fold the quartiles. For statistical significance, the Kruskal—Wallis test was used with $p = 0.05$ as a significance level. Significant differences are marked by black stars on connecting black lines for each presented box plot.

3. Results

As an initial experiment, we counted the number of parental (TGL) and brain metastatic breast cancer cells (BrM2) attached to brain endothelial cells or pericytes after 60 min of incubation. These numbers refer to the total number of cells per field of view (area) in all cases. As Fig. 3 depicts, the number of adherent tumor cells to the pericytes (HBVP) layer outnumbers those in the case of endothelial cells.

Qualitatively, for BrM2 cells larger values appear with higher frequencies, as the box is higher or the whiskers are in a higher position. Although the differences between the medians were found not significant, the distribution of the observed values might have some hints. To monitor the viscoelastic properties of the probe cell during the experiments (approximately two hours), ten-ten force curves were recorded for each immobilized cell before and after completing the measurements. In this case, the probe cell was pressed against the cell-free surface of the Petri dish. These curves provided feedback on the probe cell's viscoelastic property temporal evolution. In cases where the probe cell showed remarkably altered viscoelastic properties over time, the measurement was excluded from further analysis. Adhesive properties might be linked to elastic parameters; therefore, it would be desirable to compare the elasticity of the studied cells. Due to the measurement setup, immobilized cell as a probe on the end of a cantilever, there is no proper model available to calculate the elastic parameters of the cell. The problem becomes even more complicated when a cell is pushed to another cell.

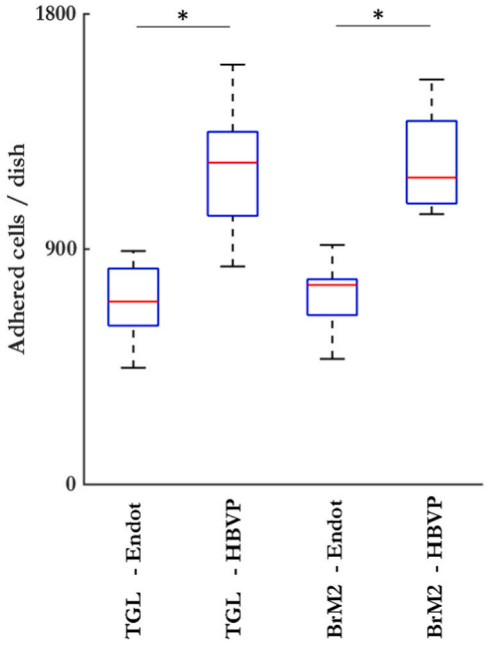

Fig. 3. Number of adherent tumor cells counted after 60 min of coculture and washout of nonattached cells. Black lines connect groups found significantly different at the $p = 0.05$ level marked with black star (*).

Despite the lack of proper models, elasticity-related parameters can be compared in the case of probe cells. Here, we present two such parameters, namely, the amount of relaxation upon the applied load and the so-called elastic index. The first one is presented in panel A of Fig. 4. This value is the percentage of the relaxation force (see panel A of Fig. 2) to the initial load. Before the probe cells were brought into contact with the target cells, ten force curves were recorded on empty areas of the dish; therefore, these curves can provide information about their initial elastic state. These values for the relaxation percentage can be seen in panel A of Fig. 4. As a first comparison, the TGL and BrM2 cells behaved in a very similar manner, and the relaxation values for BrM2 cells were shifted toward slightly larger values. This feature can be seen in the elastic index as well. In both panels of Fig. 4, higher values can be observed as the probe cell was pushed to another cell compared to when they were pushed to a hard dish surface. This suggests that the pericytes exhibit a more elastic contribution, slightly overcoming the endothelial cells.

We used six parameters to characterize intercellular adhesion: maximal pull-off force, adhesion work, and number, as well as place and instantaneous force of individual rupture events.

Fig. 5 shows the comparison of the maximal pull-off force and adhesion work of the two studied tumor cell types when pushed toward a confluent endothelial or pericyte layer successively. For both types of tumor cells, the maximal pull-off force and adhesion work are larger in the case of the pericytes than in the case of the endothelial layer.

An important parameter for characterizing cell—cell adhesion is the number of individual rupture events that occur during separation. Panel A of Fig. 6 shows a comparison of the rupture numbers in the case of endothelial cells and HBVPs when measured with both tumor cells. It can be seen that the median of the occurred rupture numbers was larger when pressed to HBVP cells.

With regard to the ruptures, the first question to be answered was whether the observed types of ruptures were due to differences in the active molecule bonds that link together during cell—cell contact. Unfortunately, the exact molecular origins could not be identified, but the size distribution of the events that occurred may indicate the types of molecular interactions.

As panel B of Fig. 6 depicts, the size distributions of the individual ruptures are almost identical for all probe cells and monitored cell layers, which suggests that very similar molecular interactions are building up the final adhesion pattern.

We can obtain a more detailed picture of the adhesion patterns between the cells if we also examine the probability distribution of where the ruptures occurred for the two tumor cell types. These distributions are shown in panel C of Fig. 6 (rupture length). From this, it can be concluded that the most frequent length of the rupture is in the range between 0.5 μm and 1.5 μm. Apart from slight shifts in the most frequent values, there were no obvious differences in the characteristics of the rupture length distribution when the probabilities are plotted.

In the case of TGL and BrM2 when in contact with HBVP, the maximum of the curve corresponding to the results shifts toward higher values. The curves obtained during contact with endothelial cells shifted toward smaller values in the case of both tumor cells. This finding also confirms that pericytes exhibit stronger adhesion. An important feature of the adhesion properties is the instantaneous rupture force probability, whose distribution can be seen in panel D of Fig. 6. This parameter can be regarded as the force needed for a rupture event to occur or the basic force that a bond can withstand for a longer period. If we compare the

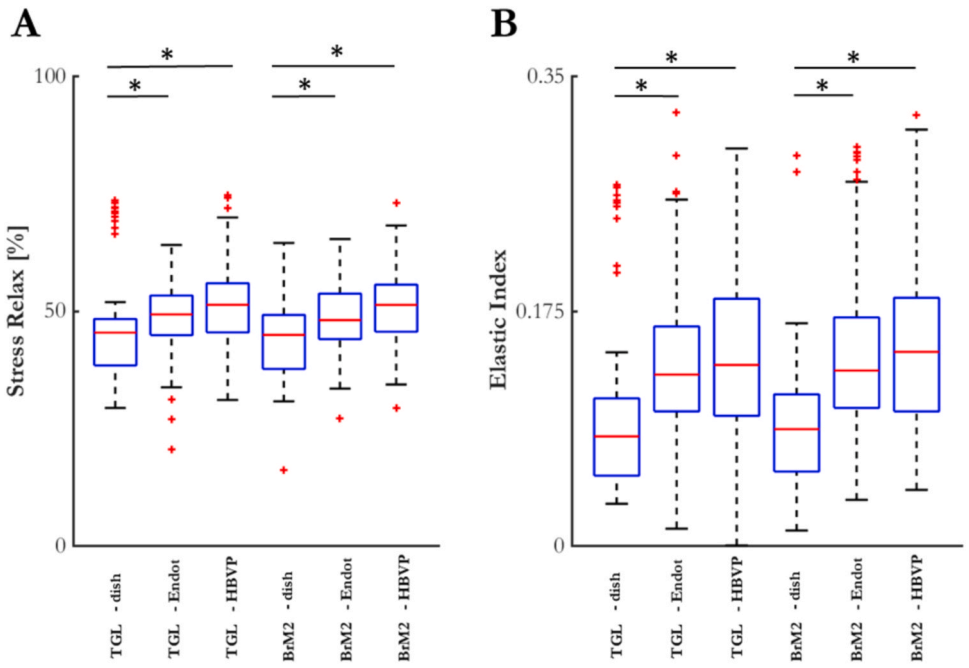

Fig. 4. Comparison of relaxation percentage (panel A) and elastic index (panel B) of the two studied breast cancer cell types (TGL and BrM2) when pushed to empty culture dish or to a confluent endothelial or pericytes (HBVP) layer successively. Black lines connect groups found significantly different at the p = 0.05 level marked with black star (*), red plus signs (+) represent outliers from distribution.

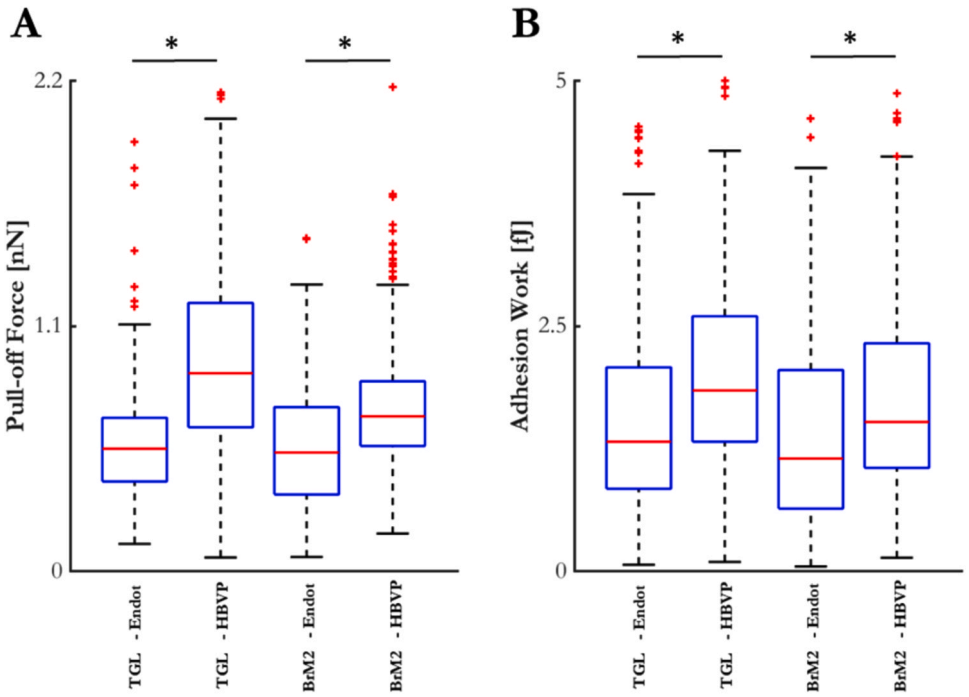

Fig. 5. Comparison of maximal pull-off force (panel A) and adhesion work (panel B) of the two studied breast cancer cell types (TGL and BrM2) when pushed to a confluent endothelial or pericyte (HBVP) layer successively. Black lines connect groups found significantly different at the p = 0.05 level marked with black star (*), red plus signs (+) represent outliers from distribution.

rupture forces between endothelial cells and the pericytes, for both sets of tumor probe-cells, the calculated probability histograms are shifted toward larger values. Pericytes excelled endothelial cells, as their ruptures occurred at larger pulling force regimes with higher probability (TGL-HBVP excelled TGL-Endot, and BrM2-HBVP excelled BrM2-Endot). In contrast, if we compared the values obtained for TGL and BrM2 cells, the values were shifted to lower regimes. TGL-Endot inferred BrM2-Endot, and TGL-HBVP inferred BrM2-HBVP. This might indicate that for BrM2 cells, ruptures at lower pulling forces occur slightly more frequently.

4. Summary and discussion

Atomic force microscopy-based single-cell force spectroscopy

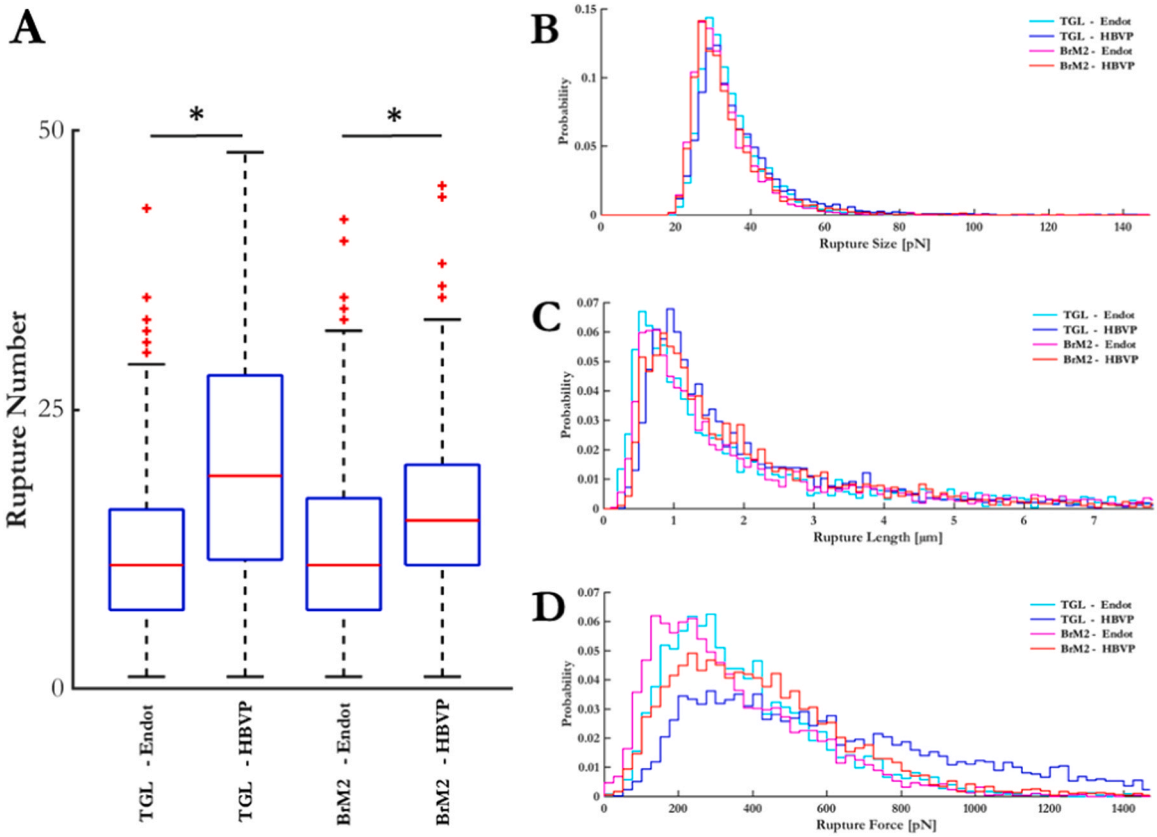

Fig. 6. Comparison of the number of rupture events per force curve (panel A), probability distributions of observed rupture sizes of ruptures per force curve (panel B), distance of occurrence from surface point (panel C) and the distribution of the pulling force values at which the identified rupture events occurred (panel D) for the two studied breast cancer cell types (MDA-TGL and MDA-BrM2) when pushed to a confluent endothelial or pericyte (HBVP) layer successively. Black lines connect groups found significantly different at the p = 0.05 level marked with black star (*), red plus signs (+) represent outliers from distribution.

provides increasingly detailed information about intercellular mechanical properties, where high force accuracy is specifically important. As brain tumors are predominantly of metastatic origin, the neurovascular unit plays a crucial role in the multistep process of colonization. Tumor cell infiltration is a prerequisite for metastasis formation, and mechanical interaction with cellular components of the neurovascular unit might also be crucial for survival. In this respect, both brain endothelial cells and pericytes are involved in the progression of metastasis formation by influencing the extravasation and survival of tumor cells [33]. Therefore, within this study, the adhesive properties of two triple-negative breast adenocarcinoma cell lines were directly measured and compared upon their contact with two basic constituents of the neurovascular unit, brain endothelial cells and pericytes. These triple negative breast cancer cells (TGL and BrM2) were characterized by Bos et. al [34]. While TGL is a parental cell line, BrM2 represents a brain-seeking variant, as it was back-isolated twice from imunodefficient mouse brain tissue, they were compared for the altered gene expressions, and a fold change of 26 genes was shown [34].

In our experiments we used an in vitro BBB model, respectively the HCMEC/D3 cell line, which maintains morphological and functional properties of brain microvascular endothelium [27] (Supplementary Fig. S1). Both the endothelial cells and the human brain vascular pericytes maintained their properties in culture. Single-cell force spectroscopy measurements were carried out in serum free Leibovitz media, which did not influence the phenotypes of these cells (Supplementary Fig. S2 panel A).

Correlation of the nanomechanical properties with metastatic potential was shown in a melanoma model [26]; however, at this time, the correlation is rather vague. In addition, comparison with literature data is very difficult for two reasons: on the one hand, there are no standardized measuring parameters; therefore, each study might use different sets (load, contact time, etc.) that do not overlap; on the other hand, the variety of cell line-related differences makes a proper comparison impossible. To the best of our knowledge, this is the first study on the direct measurement of living human tumor cell adhesion to living human pericytes. Our results show that for both tumor cell types, contact with pericytes resulted in a higher number of adherent cells after 60 min of incubation than contact with endothelial cells. Furthermore, BrM2 cells slightly but consistently outnumbered TGL cells for both endothelial cells and pericytes. Direct measurement of intercellular adhesion forces and dynamics between the investigated cell types showed further details about the adhesive patterns.

In a previous study [35], decreased adhesion forces of tumor cells with increasing metastatic potential were suggested; however, here, we need to point out that in this case, homointercellular adhesion was measured. MDA-MB-231 cells in contact with human bone marrow and pulmonary endothelial cells present slightly altered adhesion characteristics, which also depend on endothelial confluence [36]. Xie *et al.* reported direct measurements on highly metastatic breast tumor cells (MDA-MB-231, MDA-MB-435) in contact with bone marrow endothelial cells [37]. The time dependence of the deadhesion properties was monitored, concluding that adhesion occurs quicker and stronger for MDA-MB-435 cells. Here, we need to note that it is very difficult to compare our results with the aforementioned study; however, the total adhesion force between MDA-MB-435 and bone marrow endothelial cells outrages the adhesion force values of MDA-MB-231 cells in their setup. Nonetheless, there is a debate in the literature on the possible melanoma origin of the MDA-MB-435 cell line, which therefore might not be a good breast cancer model [38]. Although previous results suggested that BrM2 cells might show decreased attachment to Human

Brain-Like Endothelial Cells (BLECs) than the original MDA-MB-231 cells [39], our data (using two different methods) indicate that there is no significant difference between the adhesion properties of BrM2 and TGL cells (the proper controls of BrM2) to brain endothelial cells.

Not only the cell origin but also the surrounding environment considerably influences the fate of cells. MDA-MB-231 cells invading collagen I matrices were found to become stiffer with time [40]. Starting from this observation, we can hypothesize that those cells that are in close proximity to pericytes might behave differently compared to those in contact with endothelial cells. Upon pressing the same tumor cell to endothelial cells or pericytes, higher values were observed for both studied tumor cell types (Fig. 4) for the relaxation percentage and elastic index. Notably, to some extent, the environment might determine the adhesive parameters of tumor cells [41]. Our results suggest that pericytes constitute a more elastic environment for tumor cells.

It can be concluded that both parental and brain-seeking breast tumor cells show stronger affinity for pericytes than endothelial cells. On the other hand, brain-seeking tumor cells do not exhibit stronger adhesive properties than parental cells. Although the brain-seeking ones were found to have slightly larger elastic indexes, calculated values having a broader distribution, the adhesive characteristics seem not to be strongly related to brain affinity. This would point toward the fact that a set of other components might be crucial for their survival and prosperity within the hostile brain tissue. One of these components might be the time they are in contact with each other or even the encountered shear stress [41]. The force strength distribution where the observed ruptures occurred indicates that for brain-seeking ones, the lower force regimes are more frequent. In contrast, the contact forces of pericytes are shifted toward larger regimes, which suggests that their contacts are more stable over time. In vivo, adhesion of metastatic cells to the endothelium enables their arrest in the vessel lumen; however, as a next step, they have to migrate through the vessel wall. Therefore, the adhesion strength between tumor and endothelial cells might appear relatively low. On the other hand, strong adhesion to pericytes might be responsible for the attachment of tumor cells to the external surface of microvessels, which is essential for their survival in the brain.

CRediT authorship contribution statement

Katalin Csonti: Data curation, Writing – original draft, Investigation, Visualization, Writing – review & editing. **István A.Krizbai:** Funding acquisition, Supervision, Writing – review & editing. **Csilla Fazakas:** Conceptualization, Investigation, Visualization, Writing – original draft, Methodology, Resources, Validation, Writing – review & editing. **Kinga Molnár:** Data curation, Investigation, Resources, Writing – review & editing. **Imola Wilhelm:** Funding acquisition, Supervision, Writing – original draft, Writing – review & editing. **Attila G.Végh:** Conceptualization, Data curation, Formal analysis, Funding acquisition, Investigation, Methodology, Project administration, Software, Validation, Visualization, Writing – original draft, Writing – review & editing.

Declaration of Competing Interest

The authors declare that they have no known competing financial interests or personal relationships that could have appeared to influence the work reported in this paper.

Data availability

Data will be made available on request.

Acknowledgements

This research was funded by the National Research, Development and Innovation Office (NKFIH, Hungary; grant numbers: K135425, K135475, and TKP2021-EGA-09), the Hungarian Academy of Sciences (grant number: NAP2022-I-6), the Hungarian Research Network (HUN-REN, Hungary; project number: SA-73/2021) and the Executive Agency for Higher Education, Research, Development and Innovation (UEFISCDI, Romania; project code: PN-III-P4-ID-PCE-2020-1529). Katalin Csonti was supported by the ÚNKP-23–3-SZTE-434 New National Excellence Program of the Ministry for Culture and Innovation from the source of the National Research, Development and Innovation Fund. Csilla Fazakas was supported by the János Bolyai Research Fellowship of the Hungarian Academy of Sciences (BO/00213/19/8).

Appendix A. Supporting information

Supplementary data associated with this article can be found in the online version at doi:10.1016/j.colsurfb.2024.113751.

References

[1] X. Cheng, M.-C. Hung, Breast cancer brain metastases, Cancer Metastasis Rev. vol. 26 (3–4) (2007) 635–643, https://doi.org/10.1007/s10555-007-9083-x.
[2] L. Nayak, E.Q. Lee, P.Y. Wen, Epidemiology of brain metastases, Curr. Oncol. Rep. vol. 14 (1) (2012) 48–54, https://doi.org/10.1007/s11912-011-0203-y.
[3] J. Arnold, et al., Tubulin Tyrosine Ligase Like 4 (TTLL4) overexpression in breast cancer cells is associated with brain metastasis and alters exosome biogenesis, J. Exp. Clin. Cancer Res. vol. 39 (1) (2020) 205, https://doi.org/10.1186/s13046-020-01712-w.
[4] M. Li, N. Xi, Y. Wang, L. Liu, Atomic force microscopy for revealing micro/nanoscale mechanics in tumor metastasis: from single cells to microenvironmental cues, Acta Pharmacol. Sin. vol. 42 (3) (2021) 323–339, https://doi.org/10.1038/s41401-020-0494-3.
[5] G. Janani, M.M. Pillai, R. Selvakumar, A. Bhattacharyya, C. Sabarinath, An in vitro 3D model using collagen coated gelatin nanofibers for studying breast cancer metastasis, Biofabrication vol. 9 (1) (2017) 015016, https://doi.org/10.1088/1758-5090/aa5510.
[6] T.D. Ahrens, et al., The role of proteoglycans in cancer metastasis and circulating tumor cell analysis, Front. Cell Dev. Biol. vol. 8 (2020) 749, https://doi.org/10.3389/fcell.2020.00749.
[7] S. Valastyan, R.A. Weinberg, Tumor metastasis: molecular insights and evolving paradigms, Cell vol. 147 (2) (2011) 275–292, https://doi.org/10.1016/j.cell.2011.09.024.
[8] M. Deliorman, et al., AFM-compatible microfluidic platform for affinity-based capture and nanomechanical characterization of circulating tumor cells, Microsyst. Nanoeng. vol. 6 (1) (2020) 20, https://doi.org/10.1038/s41378-020-0131-9.
[9] S. Kumar, V.M. Weaver, Mechanics, malignancy, and metastasis: the force journey of a tumor cell, Cancer Metastasis Rev. vol. 20 (1–2) (2009) 113–127, https://doi.org/10.1007/s10555-008-9173-4.
[10] G. Guidotti, L. Brambilla, D. Rossi, Exploring novel molecular targets for the treatment of high-grade astrocytomas using peptide therapeutics: an overview, Cells vol. 9 (2) (2020) 490, https://doi.org/10.3390/cells9020490.
[11] J.F. Deeken, W. Löscher, The blood-brain barrier and cancer: transporters, treatment, and trojan horses, Clin. Cancer Res. vol. 13 (6) (2007) 1663–1674, https://doi.org/10.1158/1078-0432.CCR-06-2854.
[12] R. Harati, M.G. Mohammad, A. Tlili, R.A. El-Awady, R. Hamoudi, Loss of miR-101-3p promotes transmigration of metastatic breast cancer cells through the brain endothelium by inducing COX-2/MMP1 signaling, Pharmaceuticals vol. 13 (7) (2020) 144, https://doi.org/10.3390/ph13070144.
[13] F. Zhao, L. Zhong, Y. Luo, Endothelial glycocalyx as an important factor in composition of blood-brain barrier, CNS Neurosci. Ther. vol. 27 (1) (2021) 26–35, https://doi.org/10.1111/cns.13560.
[14] E.G. Knox, M.R. Aburto, G. Clarke, J.F. Cryan, C.M. O'Driscoll, The blood-brain barrier in aging and neurodegeneration, Mol. Psychiatry vol. 27 (6) (2022) 2659–2673, https://doi.org/10.1038/s41380-022-01511-z.
[15] Y. Li, et al., The peripheral immune response after stroke—a double edge sword for blood-brain barrier integrity, CNS Neurosci. Ther. vol. 24 (12) (2018) 1115–1128, https://doi.org/10.1111/cns.13081.
[16] E.A. van Vliet, E. Aronica, J.A. Gorter, Role of blood–brain barrier in temporal lobe epilepsy and pharmacoresistance, Neuroscience vol. 277 (2014) 455–473, https://doi.org/10.1016/j.neuroscience.2014.07.030.
[17] X. Dong, Current strategies for brain drug delivery, Theranostics vol. 8 (6) (2018) 1481–1493, https://doi.org/10.7150/thno.21254.
[18] C. Iadecola, The neurovascular unit coming of age: a journey through neurovascular coupling in health and disease, Neuron vol. 96 (1) (2017) 17–42, https://doi.org/10.1016/j.neuron.2017.07.030.
[19] P. Ballabh, A. Braun, M. Nedergaard, The blood–brain barrier: an overview, Neurobiol. Dis. vol. 16 (1) (2004) 1–13, https://doi.org/10.1016/j.nbd.2003.12.016.
[20] A. Hariharan, N. Weir, C. Robertson, L. He, C. Betsholtz, T.A. Longden, The ion channel and GPCR toolkit of brain capillary pericytes, Front. Cell. Neurosci. vol. 14 (2020) 601324, https://doi.org/10.3389/fncel.2020.601324.
[21] C.V. Carman, Mechanisms for transcellular diapedesis: probing and pathfinding by invadosome-like protrusions, J. Cell Sci. vol. 122 (Pt 17) (2009) 3025–3035, https://doi.org/10.1242/jcs.047522.

[22] K. Molnár, et al., Pericyte-secreted IGF2 promotes breast cancer brain metastasis formation, Mol. Oncol. vol. 14 (9) (2020) 2040–2057, https://doi.org/10.1002/1878-0261.12752.
[23] X. Deng, et al., Application of atomic force microscopy in cancer research, J. Nanobiotechnol. vol. 16 (1) (2018) 102, https://doi.org/10.1186/s12951-018-0428-0.
[24] J. Iturri, A. Weber, M. dM. Vivanco, J.L. Toca-Herrera, Single-cell probe force studies to identify Sox2 overexpression-promoted cell adhesion in MCF7 breast cancer cells, Cells vol. 9 (4) (2020) 935, https://doi.org/10.3390/cells9040935.
[25] A. Viljoen, et al., Force spectroscopy of single cells using atomic force microscopy, Nat. Rev. Methods Prim. vol. 1 (1) (2021) 63, https://doi.org/10.1038/s43586-021-00062-x.
[26] B. Varga, et al., De-adhesion dynamics of melanoma cells from brain endothelial layer, Biochim. Biophys. Acta Gen. Subj. vol. 1862 (3) (2018) 745–751, https://doi.org/10.1016/j.bbagen.2017.10.013.
[27] B.B. Weksler, et al., Blood-brain barrier-specific properties of a human adult brain endothelial cell line, FASEB J. Off. Publ. Fed. Am. Soc. Exp. Biol. vol. 19 (13) (2005) 1872–1874, https://doi.org/10.1096/fj.04-3458fje.
[28] C. Fazakas, et al., Transmigration of melanoma cells through the blood-brain barrier: role of endothelial tight junctions and melanoma-released serine proteases, PloS One vol. 6 (6) (2011) e20758, https://doi.org/10.1371/journal.pone.0020758.
[29] J.L. Hutter, J. Bechhoefer, Calibration of atomic-force microscope tips, Rev. Sci. Instrum. vol. 64 (7) (1993) 1868–1873, https://doi.org/10.1063/1.1143970.
[30] J.E. Sader, I. Larson, P. Mulvaney, L.R. White, Method for the calibration of atomic force microscope cantilevers, Rev. Sci. Instrum. vol. 66 (7) (1995) 3789–3798, https://doi.org/10.1063/1.1145439.
[31] M.J. Higgins, et al., Noninvasive determination of optical lever sensitivity in atomic force microscopy, Rev. Sci. Instrum. vol. 77 (1) (2006) 013701, https://doi.org/10.1063/1.2162455.
[32] A.G. Végh, et al., Adhesion and stress relaxation forces between melanoma and cerebral endothelial cells, Eur. Biophys. J. vol. 41 (2) (2012) 139–145, https://doi.org/10.1007/s00249-011-0765-5.
[33] I. Wilhelm, C. Fazakas, K. Molnár, A.G. Végh, J. Haskó, I.A. Krizbai, Foe or friend? Janus-faces of the neurovascular unit in the formation of brain metastases, J. Cereb. Blood Flow. Metab. Off. J. Int. Soc. Cereb. Blood Flow. Metab. (2017), https://doi.org/10.1177/0271678×17732025.
[34] P.D. Bos, et al., Genes that mediate breast cancer metastasis to the brain, Nature vol. 459 (7249) (2009) 1005–1009, https://doi.org/10.1038/nature08021.
[35] R. Omidvar, M. Tafazzoli-Shadpour, M.A. Shokrgozar, M. Rostami, Atomic force microscope-based single cell force spectroscopy of breast cancer cell lines: an approach for evaluating cellular invasion, J. Biomech. vol. 47 (13) (2014) 3373–3379, https://doi.org/10.1016/j.jbiomech.2014.08.002.
[36] L. Xie, Z. Sun, N.J. Brown, O.V. Glinskii, G.A. Meininger, V.V. Glinsky, Changes in dynamics of tumor/endothelial cell adhesive interactions depending on endothelial cell growth state and elastic properties, PloS One vol. 17 (6) (2022) e0269552, https://doi.org/10.1371/journal.pone.0269552.
[37] L. Xie, et al., Temporal and molecular dynamics of human metastatic breast carcinoma cell adhesive interactions with human bone marrow endothelium analyzed by single-cell force spectroscopy, PloS One vol. 13 (9) (2018) e0204418, https://doi.org/10.1371/journal.pone.0204418.
[38] J.M. Rae, C.J. Creighton, J.M. Meck, B.R. Haddad, M.D. Johnson, MDA-MB-435 cells are derived from M14 melanoma cells—a loss for breast cancer, but a boon for melanoma research, Breast Cancer Res. Treat. vol. 104 (1) (2007) 13–19, https://doi.org/10.1007/s10549-006-9392-8.
[39] A. Drolez, et al., ST6GALNAC5 expression decreases the interactions between breast cancer cells and the human blood-brain barrier, Int. J. Mol. Sci. vol. 17 (8) (2016) 1309, https://doi.org/10.3390/ijms17081309.
[40] J.R. Staunton, B.L. Doss, S. Lindsay, R. Ros, Correlating confocal microscopy and atomic force indentation reveals metastatic cancer cells stiffen during invasion into collagen I matrices, Sci. Rep. vol. 6 (2016) 19686, https://doi.org/10.1038/srep19686.
[41] B. Zhang, et al., Adhesion to the brain endothelium selects breast cancer cells with brain metastasis potential, Art. no. 8, Int. J. Mol. Sci. vol. 24 (8) (2023), https://doi.org/10.3390/ijms24087087.